Digital Image Filtering in Visualized Boundary Layers

T. C. Corke*
Illinois Institute of Technology, Chicago, Illinois

The application of two-dimensional low-pass matched filtering is presented for use in objective processing of digitized flow visualization images in order to identify instantaneous large-scale organized structures in turbulent boundary layers. The images were digitally acquired simultaneously with the outputs of a two-dimensional rake of hot-wire sensors in the field of view of the digital camera. Two-dimensional low wavenumber analysis brought out patterns in the visualization images which consisted of slender inclined structures having an average streamwise scale of 100-200ν/u_τ and a length on the order of $1-2\delta$. The similarly processed two-dimensional streamwise velocity reconstructions reveal similar features. The ensemble statistics indicate that these inclined features brought out by this processing may be a basic flow module in higher Reynolds number flows which links the so-called wall "bursting" process and the larger outer scale motions.

Introduction

IN the last 20 years, the research on turbulent boundary layers has transformed the picture given by earlier long-time average statistics. This revolution in thinking was set forth primarily by Townsend[1] and Grant[2] who, while being interested primarily in turbulent wake flows, viewed the turbulent flowfield as one where turbulent fluid is moved about by motions of a system of large coherent eddies whose dimensions scaled with the width of the flow. Townsend,[1] in particular, inferred from velocity correlation measurements the presence of characteristic eddies of finite length with a structure inclined in the flow direction. Later, Townsend[3] described these structures as an inclined pair of double-roller eddies, a picture which was consistent with the eddy pattern perceived by Grant.[2] In the 1967 paper by Kline et al.,[4] the then new hydrogen bubble visualization technique revealed the presence of surprisingly well-organized motions in the near-wall "streaks" which eventually interacted with the outer portions of the flow through a process "of gradual lift-up, sudden oscillation, bursting and injection." This sequence of events later became known as "bursting." It is felt that this process played an important and dominant role in the production of new turbulence and the transport of turbulence away from the wall. As a result of the work by Blackwelder and Kaplan,[5] the overall burst process has sometimes been associated with a rapid deceleration/acceleration on the near-wall streamwise velocity, although this velocity signature accounts for only one part of the process originally depicted by Kline et al.[4]

Since the measurements of Corrsin and Kistler[6] of intermittancy in the outer parts of the boundary layer, it became clear that the turbulent/nonturbulent interface extends well into the boundary layer. The studies of intermittancy by Fiedler and Head[7] gave visual evidence of this. Kovasznay,[8] utilizing conditional sampling techniques, defined "fronts" and "backs" to these turbulent "bulges." From velocity correlations, Blackwelder and Kovasznay[9] later defined a mean motion inside a turbulent bulge which was rotational with a mean vorticity component in the same direction as the mean strain rate. From their measurements, they estimated that these large eddies contribute as much as 80% of the Reynolds stress for $y>0.2\delta$. The conditioned measurements of Antonia[10] were in substantial agreement with them. In addition, he determined that the maximum $\overline{uv}$ distribution within the turbulent bulges represents approximately 45% of the wall shear value.

On the trailing backs of the large-scale eddies, Falco[11] noticed predominant small-scale eddies, with sizes on the order of 100 to 200ν/u_τ which he associated with the Reynolds stress-producing motions. Head and Bandyopadhyay[12] present a picture of the large eddy structures as being an amalgamation of elongated hairpin vortices. These hairpins have a preferred inclination angle of 45 deg to the wall. It was suggested in Ref. 12 that Falco's[11] small-scale eddies are actually tips of these hairpin eddies. Chen and Blackwelder,[13] through the use of thermal tracing, brought out the existence of an internal shear layer which they found to lag slightly behind the velocity signals they associated with the bursting phenomenon. Brown and Thomas[14] suggested, based on correlation measurements, that an organized structure at an oblique angle of 18 deg and of order 2δ long, might be a coherent flow module in the turbulent boundary layer.

In spite of the well-established existence of these large-scale motions, the mechanisms for their generation are still in question. Zilbermann et al.[15] and Wygnanski[16] generated turbulent "spots" in a transitional boundary layer and followed their development downstream. They concluded that the turbulent spots were related to the large-scale motion in a turbulent boundary layer. Previously, Coles and Barker[17] had suggested that the turbulent spot is the basic building block of the turbulent boundary layer. Taking the lead of Klebanoff,[18] Head and Bandyopadhyay suggest that the more basic structural element of a turbulent boundary layer is the hairpin eddies observed in the transition process.

In light of the fundamental questions that remain unanswered about the coherent process that have been observed to play a major role in the growth and evolution of a turbulent boundary layer, we undertook an experiment which was designed to separate the inner and outer coherent motions and point to mechanisms of their interaction, growth, and decay. This involved altering the outer part of the turbulent boundary layer by suppressing the large-scale intermittant outer bulges. We then documented comparisons of the mean and unsteady aspects of these turbulent boundary layers. In this paper we choose to emphasize the unsteady aspect of those flowfields through the use of simultaneous acquisition of the outputs from a rake of velocity sensors and the digitized view of the flowfields made visible using the "smoke-wire" technique (Corke et al.[19]). These image and velocity data

Presented as Paper 83-0379 at the AIAA 21st Aerospace Sciences Meeting, Reno, Nev., Jan. 10-13, 1983; submitted Jan. 31, 1983; revision received Aug. 12, 1983.

*Assistant Professor, Mechanical Engineering. Member AIAA.

arrays were specially processed using two-dimensional "matched" filtering in order to bring out the "coherent" features so as to discern what, if any, fundamental flow modules may be statistically linked to the generation of turbulent stresses in the near-wall region of the flow.

Two-Dimensional Processing

The digital processing of images requires that the visualized flowfield be discretely sampled, digitized, and stored on some media such as digital magnetic tape or disk. This was accomplished with the use of a EMR Photoelectric model 659F optical data digitizer which was interfaced to a PDP-11 bus. The camera incorporates a Vidicon imaging tube which stores an electron charge pattern proportional to the luminous energy of an image focused on the tube. As contrasted with a scanning type video tube in which the image data is retrieved by sequential sweeps, the Vidicon tube has 4096×4096 randomly addressable picture elements (pixels) from which the monochromatic intensity information can be retrieved. As a result of some spatial averaging of adjacent pixels, the number of resolvable points for the tube is 512×512. The analog intensity information is converted to an 8-bit parallel binary intensity word through an A/D converter in the camera. This gives 256 resolvable levels of intensity. Since the PDP-11 word is two 8-bit bytes the image data were packed into double bytes to reduce storage requirements. The Vidicon tube is sensitive to light energy in the range of 10^{-6}-10^{-4} ft-c-s which gives an equivalent Film ASA rating of approximately 3000. All operations of the camera and data transfer were controlled by the host PDP-11 processor through Fortran callable assembly language subroutines.

The intent of this portion of the paper is to outline a methodology for objectively discerning coherent features that might exist in recorded realizations of visualized flowfields. As an aid to the reader, these steps are demonstrated through the use of synthetic data of known spatial content. In Fig. 1, the letters IIT represent a complex, quasirepeating spatial function. In order to simulate conditions that would exist in visualized turbulent flows, where we have coherent features with superimposed, incoherent fine scales, Gaussian noise was added into the intensity field as shown in the bottom part of the figure. The additive noise in this example had an amplitude corresponding to 80% of the intensity amplitude of the letter pattern yielding a signal-to-noise ratio of 1.25. The included "color" bar provides the gray level correspondence to the pixel intensity value in the range from 0(black) to 255(white).

Two-dimensional pattern recognition was performed on the noisy image to obtain an unbiased reconstruction of the low wavenumber features. This is in contrast to other nonclassical (in an electronics signal processing sense) "pattern recognition" schemes such as used by Wallace et al.[20] which have a different statistical basis. Here, the pattern recognition was accomplished by match filtering the image with a two-dimensional low-pass filter function. The general use of bandpass filters in match filtering has the advantage of more controlled enhancement of specific scales of features without any pre-bias on their translational or rotational orientation. This approach can be contrasted to that of Townsend[21] and Mumford[22] who both utilized specific "model" velocity patterns.

One-dimensional low-pass linear phase finite impulse response (FIR) filters were designed for this experiment using a program written by McLellan et al.,[23] which is one of a number of programs for processing of digitized signals. The weighting and stop band cutoff frequencies were designed to give a minimum amount of ripple and the greatest amount of amplitude cutoff. In typical designs utilized on the images, the amplitude in the stop band was reduced by 60 dB.

The impulse response of the one-dimensional filter function was subsequently mapped into a two-dimensional circularly symmetric response by the function

$$\cos(2\pi f) = 0.5\cos(2\pi f_1) + 0.5\cos(2\pi f_2) + 0.5\cos(2\pi f_1)\cos(2\pi f_2) - 0.5$$

where f_1 and f_2 are the two frequency components in the two-dimensional mapping plane. Rabiner and Gold[24] show that this transformation results in a two-dimensional linear phase approximation which is optimal in a Chebyshev sense. The match filter has an impulse response equal to the space-reversed version of the filter response to which it is matched so that the response is identical to an autocorrelation function. The peak in the autocorrelation, marking the match, occurs at a zero lag time and is proportional to the total energy of the signal waveforms. It can be shown theoretically[25] that the improvement in signal-to-noise ratio caused by a match filter is the best possible.

The process was achieved by performing a two-dimensional discrete Fourier transform on the image and match filter. The convolution is performed in wavenumber space where it is equivalent to complex multiplication. This approach is more computationally efficient when dealing with arrays larger than 4×4. In order to eliminate the circular effect in the time-limited autocorrelation function, the image was space extended to twice its original size with zeros. In the event that an image is processed in segments, a continuous transition between parts is accomplished using an overlap-add method, which accounts for the fact that the linear convolution of each section with the sample response is larger than the sample space. Adjacent segments are overlapped by an amount equal

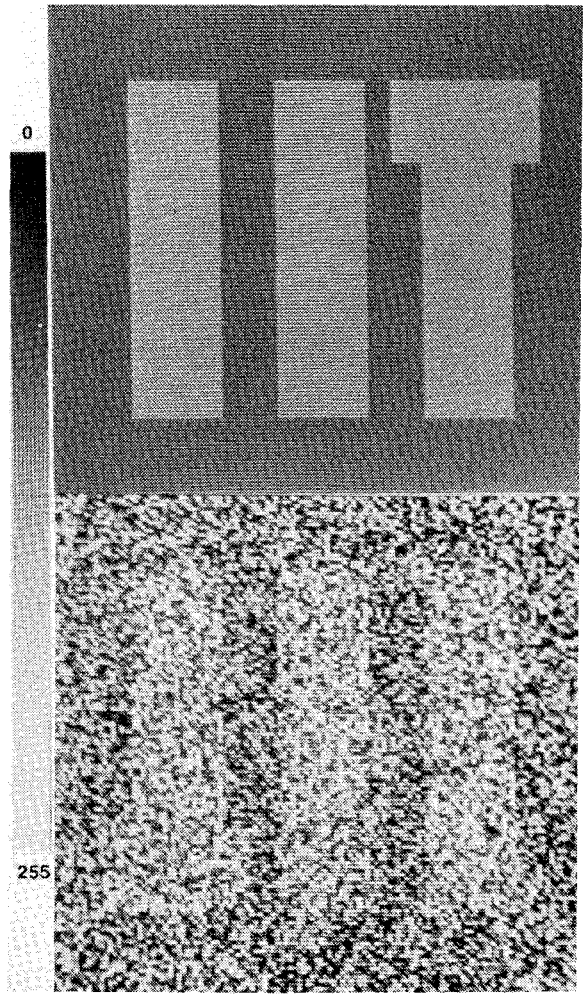

Fig. 1 Gray level representation of image array of letters IIT without and with 80% additive noise.

to the filter width. Further details are contained in the reference by Corke.[26]

The result of the match filtering of the test data is shown in Fig. 2. Comparing the result with the original in Fig. 1 demonstrates the degree of reconstruction.

Experimental Methods

The experiment was performed in the high-speed test section of the Mark Morkovin wind tunnel. The tunnel runs in a closed-return configuration with the return leg being used for atmospheric boundary-layer simulations. In the high-speed section, honeycombs and screens upstream of a 4:1 contraction give a turbulence intensity level of 0.03% over a range of velocities from 1 to 30 m/s. The rectangular test section is 0.61 m wide × 0.91 m high × 4.88 m long with plexiglass back and front side-walls to allow for easy flow visualization. A 5.16-m-long flat plate served as the boundary-layer plate for the experiment. To be able to place the plate inside the test section, it was fabricated in three parts with lengths 1.68, 1.85, and 1.63 m, respectively, from the leading edge. This arrangement is shown in the schematic in Fig. 3.

The first plate section was fabricated from a 1.6-cm-thick aluminum plate. The leading edge was machined to a razor edge and sloped downward so as to fix the stagnation point on the measurement side of the plate. The two other sections were made from 1.3-cm-thick clear plexiglass which was mounted to a metal fram made from 2.5-cm square aluminum channel to maintain a flat surface. Each plate section was suspended on four independently adjustable legs. This partitioned the test section so that a 0.61 × 0.61-m square cross section was formed above the plate. The seams between the three plates were glued together, covered with plastic filling compound and wet sanded to provide a smooth, flush surface. A slightly higher pressure was maintained on the measurement side of the test section by placing a 40% solid perforated plate at the downstream end across the part of the test section above the plate. This ensured that the stagnation streamline impinged on the downward sloping leading edge, as verified with smoke wire visualization. The sand paper at the leading was utilized as a "transition trigger." That is, it fixed the point of transition to turbulence at a downstream location off the sandpaper, which was insensitive to any outside disturbances.

Fig. 2 Matched filtered result of noisy image of Fig. 1 (gray level mapping same as in that figure).

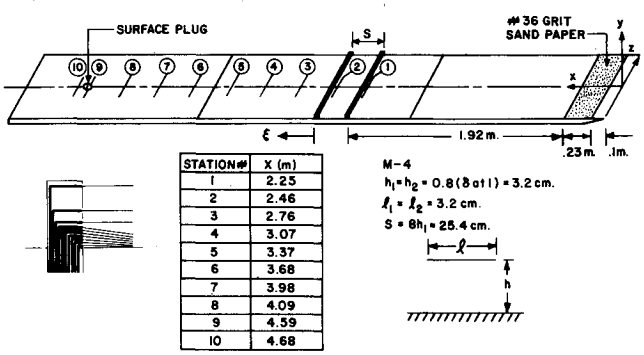

STATION#	X (m)
1	2.25
2	2.46
3	2.76
4	3.07
5	3.37
6	3.68
7	3.98
8	4.09
9	4.59
10	4.68

Fig. 3 Schematic of boundary-layer plate showing measurement stations and two tandem manipulator plates.

Included in the schematic in Fig. 3, is a representation of the boundary-layer large-scale "manipulator" as well as its placement and dimensions. The dimensions and placement of this as well as other manipulators was chosen through an optimization process by visually observing the degree of suppression of the large intermittant outer scales in the flow. The details of this study are included in the paper by Corke and Nagib.[27] The manipulator consisted of two 0.2-mm-thick brass plates in the tandem arrangement shown in Fig. 3. The chord of each of the plates and its elevation above the wall was equal to 80% of the boundary-layer thickness. The two plates were spaced 25.4 cm apart or eight times the boundary-layer thickness at the upstream plate. The manipulator plates were held under tension at either end of the test section. Special care are taken to make sure that the plates were not sagging, twisted, at an angle of attack, or vibrating under operating conditions.

The simultaneous acquisition of the rake of 10 wires, the shear wire, and the digitized image of the smoke-wire visualized flowfield was designed to look in detail at the relationship between the large-scale outer structures and the wall burst mechanism in the turbulent boundary layers. The design of the probe concentrated as many as seven sensors below $y^+ = 100$, which has been observed to bound the influence of the wall events. Although other sensors as high as $y^+ = 800$ would provide some information about the large-scale turbulence, the digital images, viewing the whole boundary layer over a number of boundary-layer thicknesses, would be used primarily for that information.

The method by which the data was acquired reflects the type of information we wanted to extract and the limitations of the equipment. For example, we wanted the sampling rate to be fast enough to give sufficient resolution of points during a burst event and to be continuous for a sufficient amount of time to ensure more than one event per sampling record. For a number of statistically independent samples, the first criterion was limited only by the speed of the A/D converter and controlling assembly language software. For 13 input channels a maximum sequence sampling rate of approximately 2000 Hz could be attained. The second criterion was limited by sampling rate and the amount of computer memory available. Since the 65 K bytes of image data could not be retrieved from the digital camera fast enough to keep pace with the hot-wire acquisition, only one image per sampling was possible. Therefore, the images had to be "conditioned" on the event. Since we wanted the images and hot-wire data to coincide, the detection of the event had to also initiate the hot-wire acquisition. However, we were also interested in the pre-event history of the flow. The acquisition strategy was designed to allow for all these requirements.

The results of Rao et al.,[28] Laufer and Narayanan,[29] Blackwelder and Kaplan,[5] and others have suggested that in the range of Reynolds numbers of this investigation the nondimensional period between burst events is $TU_\infty/\delta \simeq 5$. In the case of the low Reynolds number regular boundary layer, a sampling frequency of approximately 1800 Hz would resolve this period into 100 points. Approximately 400 words of memory were available to store each of the 11 channels of anemometer outputs, temperature, and pressure so that at this

sampling rate an average of four events could be detected. The acquisition rate was adjusted to maintain this resolution over the range of boundary-layer parameters.

The analog signal output of channel 10 of the anemometer was used to detect the burst events. This signal, which was proportional to the instantaneous velocity at $y^+ = 7$ in the boundary layer, would be examined for occurrences of a local high variance compared to the long-time background values. Although it has been common for investigators to use a sensor at $y^+ = 15$, the results by Blackwelder and Kaplan[5] show that the velocity signature of these events remains coherent in the whole portion of the boundary layer below $y^+ = 100$. The signal at $y^+ = 15$, being near the peak in the vertical distribution of turbulence intensity, has considerably more turbulence fluctuations thereby making the detection more difficult. The VITA technique (Blackwelder and Kaplan[5]) in effect low-pass filters the velocity data to perform the detection. However, in this case, analog filtering would be undesirable since it would introduce a phase shift in the detection signal. The signal from the $y^+ = 7$ sensor allowed easy detection without low-pass filtering.

The anemometer output of the detection wire was linearized with a DISA 55D10 linearizer and input to a DISA 55D35 rms meter to measure the long-time average rms and to output a signal proportional to the instantaneous variance. The analog signal was fed to the variable threshold level detection circuit. The output from the level detection circuit consisted of a transistor-transistor-logic (TTL) logic status corresponding to

$$\text{Condition} = 0 : u'^2_{10} < k\overline{u'^2_{10}}$$

$$= 1 : u'^2_{10} \geq k\overline{u'^2_{10}}$$

where k is an adjustable threshold coefficient. The logic output was connected to the condition logic in the smoke-wire control. Although this simple threshold dependent criteria was used in the acquisition of the images, only those realizations that passed a more objective match correlation criteria were selected as part of the ensemble result.

The smoke-wire circuit is made up of timing chips which control the duration of heating of the wire and the delay needed for the smoke to be convected into the field of view before triggering a camera and/or strobe light. In addition, digital logic in the circuit allows photographs to be taken when the smoke is in view and when an external condition is satisfied. The conditioned photographs are necessary to do ensemble image averaging. The instrumentation schematic for the simultaneous acquisition of the digitized image and hot-wire rake output is shown in Fig. 4.

The experiment was run in a darkened lab so that the image was recorded at the instant of the strobe flash. The flash is approximately 1 ms in duration which was sufficiently short to "freeze" the motion of the smoke image. In order to be able to mark that instant on the sequence of data, the trigger output pulse was multiplexed onto the slowly varying signal proportional to the wind tunnel air temperature, which was used for compensating the anemometer outputs for mean temperature variations.

The digital camera, which was mounted on a tripod, was connected to the PDP-11 bus through the merging logic unit and DR11-C interface. Under software control, the camera was operated at the 30-Hz scanning mode while the D/A outputs of the camera were viewed on a Tektronix 604A black/white monitor which sat on top of the camera. During this operation, the camera performed like a conventional television camera which made it easy to position and focus. For both of the low Reynolds number boundary-layer cases the camera was set up to record two views of the flow. One view (zoomed out) encompassed approximately eight boundary-layer thicknesses and utilized a 50-mm f:1.4 lens. The other (zoomed in) encompassed approximately two boundary thicknesses and utilized a 210-mm f:3.5 macro/zoom lens. In both cases, the rake of hot wires was visible in the image. The camera was not moved throughout this phase of the acquisition. To be able to compare the image results with future data runs, the camera always viewed two LED lamps which were precisely spaced to provide a scale. During the retrieval and storage of the image data, the digital numbers were copied into the MDP-3 display processor graphics memory and displayed on the Conrac 5211C color display monitor. The MDP-3 graphics memory was also used for temporary storage of the digitized 13 channels of data.

The acquisition was directed by the PDP-11/04 processor as controlled by the acquisition software. The timing diagram for the simultaneous acquisition is shown in Fig. 5. After the smoke wire is coated with oil, the sequence is initiated by a keyboard command. Prior to this, the digital camera is in a prime mode which erases any previous images. A start pulse is sent to the smoke-wire control circuit to begin the generation of the smoke streaklines. The duration of the smoke and the delay time to allow for the smoke to be convected had been preset in the smoke-wire control. It is within this "window"

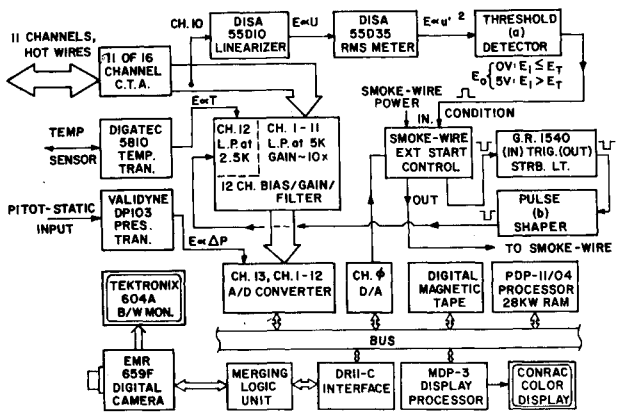

Fig. 4 Schematic of instrumentation used in simultaneous acquisition of output from hot-wire rake and digital camera.

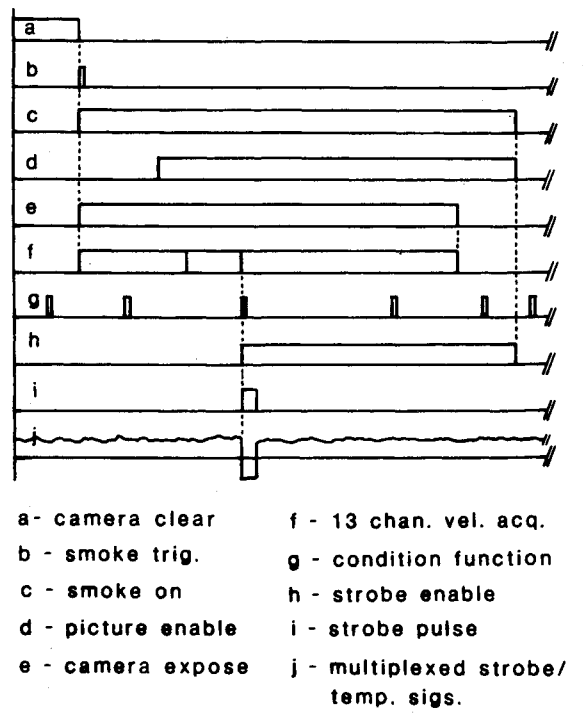

Fig. 5 Timing diagram for conditioned acquisition of outputs from hot-wire rake and digital camera.

of time that the smoke is in the field of view and during which we search for a condition. The window was typically 1-2 s wide. The condition is only valid if it occurs when the smoke is in view.

Since we do not know a priori where in this window an event will occur, the acquisition of the 13 channels began at the initiation of the sequence and the data were stored in computer memory. For the sampling rates used, the amount of available data storage was too small to accommodate the time interval within our conditional window. Therefore, the software configured the space into a "circular" buffer so that old data were overwritten. Between each sequence of 13 channels, and before the next interrupt of the programmable clock, the data value of channel 11 of the A/D was checked to see if the condition, marked by a -10 V pulse, had occurred. If the condition was detected, 50 points, or one half of an average burst cycle, preceding the event were kept and the remaining 350 points following the event were acquired to fill the buffer. Also, at the instant the condition occurred, the strobe flashed and the smoke image was stored on the digital magnetic tape. The camera was subsequently put in the prime mode awaiting the next sequence.

Depending on the delay time allowed for the convection of the smoke, it was possible that 50 points were not acquired before an event was detected. In such a case the data set was discarded. It was also possible that no events be detected inside the window. In this case, the acquisition loop was reset manually and the data was discarded.

The threshold for the detection was set using a Hewlett Packard (HP) digital spectrum analyzer. The output of the threshold detector circuit was connected to the external trigger input of the spectrum analyzer to conditionally sample the events. The threshold was raised until the educted ensemble average resembled the signature for the burst process. The ratio of the instantaneous threshold variance level to the long-time average variance used in the regular and manipulated boundary layers was 3.5. This number is not to be confused with the threshold used in the VITA technique since those values are the local average over $10Tu_\tau^2/\nu$ points.

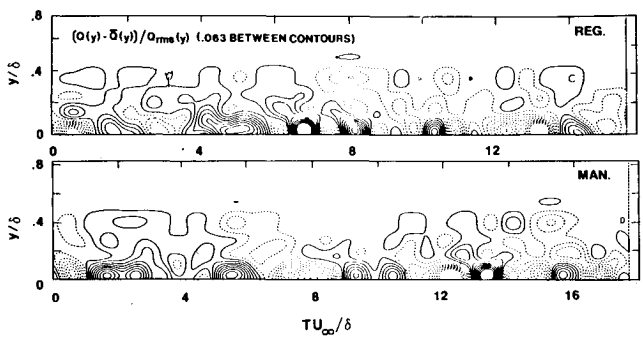

Fig. 6 Two-dimensional filter reconstruction of normalized streamwise velocity time series for boundary layers without (top) and with suppression of large-scale intermittancy.

Image Processing in Boundary Layers

Although the emphasis of this paper is on the unsteady aspects of the turbulent boundary layers, considerable documentation of the time-mean characteristics of these flowfields was made in order to ensure their quality and repeatability. These results, which are presented in the paper by Corke and Nagib[27] include profiles of the first four moments of the streamwise velocity component, integral boundary-layer thicknesses, shape factors, the streamwise distribution of the wall friction coefficient and mean entrainment velocity, one-dimensional velocity spectrums, autocorrelations, and integral length scales.

As in the case of the digitized images, the outputs of the rake of sensors can be treated as a two-dimensional array. By this arrangement, the vertical space coordinate of the sensors forms one sampling dimension and the Eulerian time frame the other sampling dimension. In this frame work, the two-dimensional velocity surveys can be processed in an identical way as that of the images (outlined in the section on Two-Dimensional Processing). In order to properly represent the relative different spacings between the sensors, zeros were inserted between discrete vertical sampling locations in the array. The largest spacing between sensors provides the upper spatial frequency limit for the reconstruction of the space-time velocity field. A two-dimensional symmetric low-pass filter was designed for this application. The cutoff frequency was chosen for this application as well as for the images so as to pass turbulent scales with lengths less than or equal to approximately $100\nu/u_\tau$. This appeared to be a reasonable value given the average length scales of coherent motions available in the literature due to Kline et al.[4] ($\sim 100\nu/u_\tau$), Falco[11] ($\sim 200\nu/u_\tau$), Brown and Thomas[14] ($\sim 100\nu/u_\tau$), and, most recently, Head and Bandyopadhyay[12] ($\sim 100\nu/u_\tau$). It is, however, a trivial matter to reprocess the data using higher frequency cutoffs should the need arise.

In Fig. 6 is shown one realization of the space-time velocity reconstructions for the boundary layer with and without suppression of the large intermittant outer scales. The velocity values are presented as constant value contours of the instantaneous fluctuating quantities normalized by the local average rms. This quantity represents a measure of the fluctuating intensities which stand out above the background turbulence fluctuations. Coherent amalgamations of these indicate "structures" in the turbulence. In Fig. 6, the solid contours denote regions of positive normalized velocity, that is, with velocities greater than the mean. The dashed contours denote regions of negative normalized velocity. The burst process defined by Blackwelder and Kaplan,[5] which consists of a velocity signature made up of a rapid deceleration/acceleration, would correspond to adjacent dashed solid

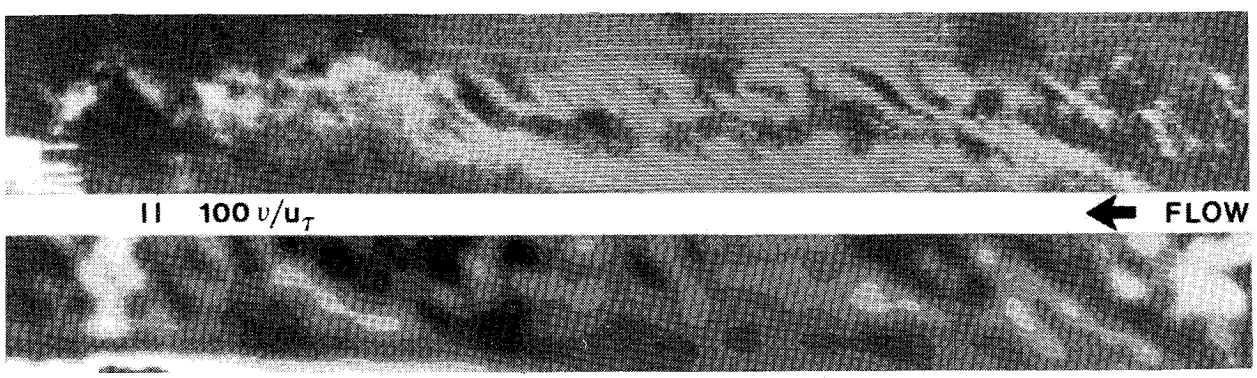

Fig. 7 Digital realization of visualized flow conditioned on wall "event" (top) and corresponding matched filtered representation (bottom) in boundary layer without suppression of large-scale intermittancy.

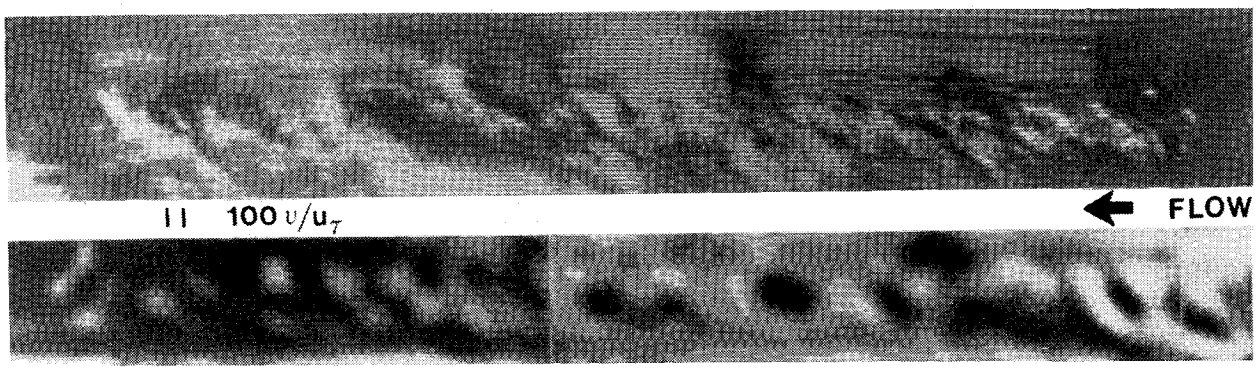

Fig. 8 Digital realization of visualized flow conditioned on wall "event" (top) and corresponding matched filtered representation (bottom) in boundary layer with suppression of large-scale intermittancy.

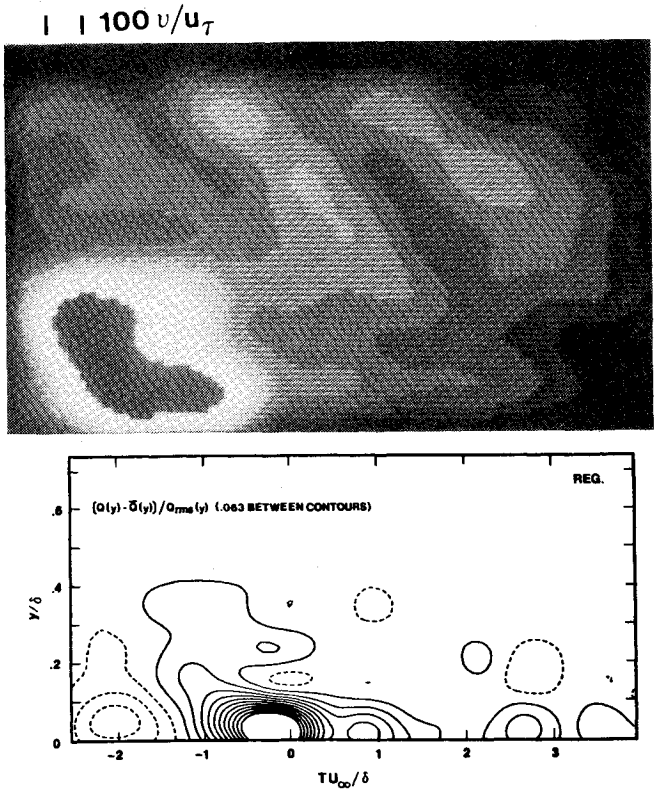

Fig. 9 Ensemble average of matched filtered images conditioned on wall "event" and filtered streamwise velocity in boundary layer without suppression of large-scale intermittancy.

features in the contour representation in Fig. 6. In the contours of that figure, the acquisition was initiated by the real-time detection of the burst event which is visible as the dashed-solid pair centered at $TU_\infty/\delta = 1$. Further inspection strongly suggests that the velocity field near the wall is in a constant state of acceleration and deceleration. In fact, it looks like a bistable mode of the near wall flow. This behavior is reminiscent of the model for the wall layer proposed by Black,[30] Einstein and Li,[31] and Hanratty[32] who considered the flow to be in a constant state of dissipation and regeneration. The frequency of these motions has been correlated with the boundary-layer parameters (see Corke and Nagib[33]).

Since the rake of sensors only spans the boundary layer up to $y^+ = 500$, we look to the processed visualization records to view the total bulk of the flow. Gray level representations of two typical realization of digitized images are shown in the top half of Figs. 7 and 8 for the boundary layer without and with the suppression of outer intermittant scales, respectively. In this representation, black corresponds to the minimum reflected light intensity and white corresponds to the maximum intensity. The view shown in these figures covers approximately eight boundary-layer thicknesses, where the rake of sensors appears at the extreme left. The outer intact streaklines emanating from the smoke-wire mark the potential flow and the turbulent/nonturbulent interface. Shown for reference on these figures is the scale indicating $100\upsilon/u_\tau$.

The lower halves of the figures correspond to the match filtered reconstructions of the digitized images in Figs. 7 and 8. Here, black corresponds to a low match correlation and white corresponds to a high correlation. The rake of sensors has been digitally removed from these processed images as well as any nonuniformities due to lighting and camera spatial sensitivity. If we focus on the sample realization in Fig. 7 for which there was no suppression of the outer intermittant scales we note the long slender features inclined on the flow direction. Although there seems to be a fairly wide distribution of inclination angles, those features which extend across the total height of the boundary layer seem to be inclined in the vicinity of 45 deg. In the vicinity of the rake of sensors, where the detection of a wall burst initiated the image acquisition, we observe a more closely packed and regular arrangement of these 45-deg features. To determine if these are statistically related to the wall event we will look to the ensemble averages results to follow.

In the realization for the boundary layer where we suppressed the outer intermittant scales, there appears to be a more regular pattern of these 45-deg features. In these boundary layers the local skin friction has been lowered by approximately 30% through the suppression of the large-scale intermittancy. It is speculated by Corke and Nagib,[27] that these manipulated boundary layers emulate higher Reynolds number flows with equivalent Re_θ's of approximately 21,000. That is, that the large-scale intermittancy is due to the decaying remnants of transition spots. By suppressing these motions, we have "aged" the boundary layer in a Reynolds number sense. The lower drag is one manifestation of this. These features brought out by the image processing may be the characteristic structure in these higher Reynolds number flows. Head and Bandyopadhyay[12] give evidence that this is the case.

The phase conditioned ensemble average of enhanced images are shown in Figs. 9 and 10 for the boundary layers without and with the large-scale suppression. In this presentation the rake of sensors appears in the bottom left of the image. The dominant feature which is correlated with the burst event in both boundary-layer flows is the 45-deg inclined patterns observed in the long views in Figs. 7 and 8. The local maximum (bright spot) at the outer tip of the feature indicates that the smoke was rolled up in that region suggesting a possible eddy structure. This may very well be a visual ensemble of a streamwise cut through hairpin-like vortices. In

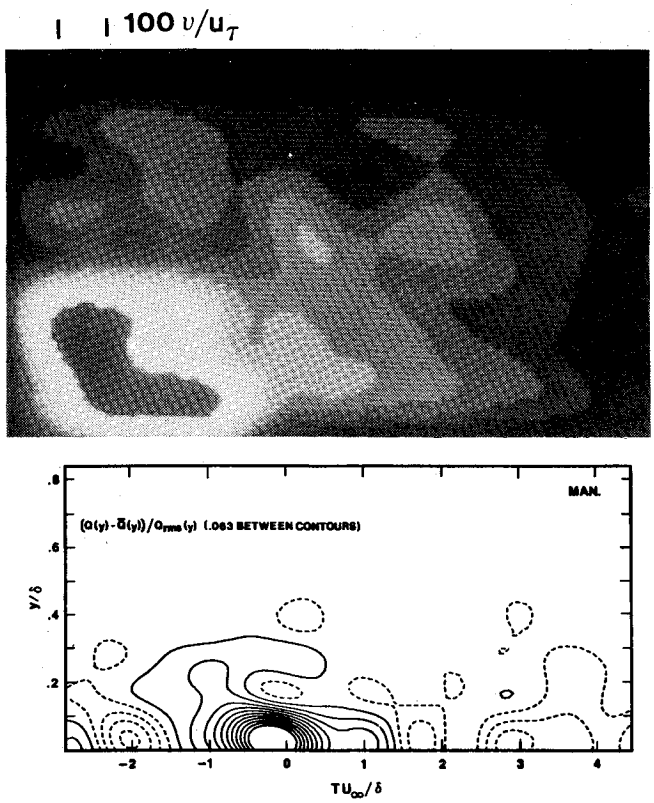

Fig. 10 Ensemble average of matched filtered images conditioned on wall "event" and filtered streamwise velocity in boundary layer with suppression of large-scale intermittancy.

the manipulated boundary layers the ensemble feature is shorter owing to the thinning of the boundary layer which accompanies the suppression of the large-scale intermittancy.

The ensemble averages velocity reconstructions in the bottom portions of Figs. 9 and 10 present a picture which is consistant with the images, that is, of an inclined lifted feature. Note that the rake of sensors only extends up to approximately 40% of the mean boundary-layer thickness and, therefore, indicates features in the lower part of the images. It is interesting to note that the feature having the highest coherence (brightest) in the ensemble average of the processed images resides at the streamwise position slightly upstream of the velocity sensors at the instant of a wall "event," $TU_\infty/\delta = 0$. This observation might account for the Eulerian time lag observed by Chen and Blackwelder[13] between the velocity signature they associated with the burst event and the passage of the thermally tagged shear front. The images for both boundary-layer types, however, clearly shows a succession of these 45-deg features in the ensemble average.

It is perhaps premature to speculate on the origin of these features brought out in the images, however, the similarities in the scales and orientation to the visualized structures observed by Head and Bandyopadhyay[13] are striking. If, as they suggest, these features are hairpin vortices, then they are a statistically significant flow module which is linked to locally high-velocity stresses in the region of high-turbulence production near the wall. It is apparent from the results that features on the scale of the turbulent spot (~ 10 times larger) are not predominant to the flow at these Reynolds numbers. Although the view that a turbulent spot is an amalgamation of hairpin eddies is not ruled out, that would make the spot somewhat of a substructure to the flow, most likely only important in the early development of the turbulent boundary layer.

Concluding Remarks

The application of matched filter processing was demonstrated for more objective detection and description of two-dimensional features in digitized images and velocity fields. In its application in turbulent boundary layers, it revealed extended features 1 to 2 boundary-layer thicknesses in length which were inclined at a mean angle of 45 deg. Their mean streamwise width was approximately $100v/u_\tau$. Although the evidence suggests that these features are the result of "hairpin" vortices emanating from the wall, future experiments, in which the flow is viewed in all three dimensions, are needed to verify this result. In that case the methods presented here can be extended easily.

Acknowledgment

The author would like to thank Judy Siuciak for typing the manuscript. This work was sponsored under NASA-Langley Research Center Grant NSG-1591.

References

[1] Townsend, A. A., *The Structure of Turbulent Shear Flow,* Cambridge University Press, 1956.

[2] Grant, H. L., "The Large Eddies of Turbulent Motion," *Journal of Fluid Mechanics,* Vol. 4, Pt. 2, June 1958, pp. 149-190.

[3] Townsend, A. A., "Entrainment and the Structure of Turbulent Flow," *Journal of Fluid Mechanics,* Vol. 41, Pt. 1, March 1970, pp. 13-46.

[4] Kline, S. J., Reynolds, W. C., Schraub, F. A., and Runstadler, P. W., "The Structure of Turbulent Boundary Layers," *Journal of Fluid Mechanics,* Vol. 30, Pt. 4, Dec. 1967, pp. 741-773.

[5] Blackwelder, R. F. and Kaplan, R. E., "One the Wall Structure of the Turbulent Boundary Layer," *Journal of Fluid Mechanics,* Vol. 76, Pt. 1, July 1976, pp. 89-112.

[6] Corrsin, S. and Kostler, A., "The Free Stream Boundaries of Turbulent Flows," NASA TN 3133, 1954.

[7] Fiedler, H. and Head, M. R., "Intermittancy Measurements in the Turbulent Boundary Layer," *Journal of Fluid Mechanics,* Vol. 25, 1966, p. 719.

[8] Kovasznay, L. S. G., "Structure of the Turbulent Boundary Layer," *Physics of Fluids,* Vol. 10, Sept. 1967, Suppl., pp. 25-30.

[9] Blackwelder, R. F. and Kovasznay, L. S. G., "Time Scales and Correlations in a Turbulent Boundary Layer," *Physics of Fluids,* Vol. 15, No. 9, Sept. 1972, pp. 1545-1554.

[10] Antonia, R. A., "Conditional Sampled Measurements Near the Outer Edge of a Turbulent Boundary Layer," *Journal of Fluid Mechanics,* Vol. 56, Pt. 1, Nov. 1972, pp. 1-18.

[11] Falco, R. E., "Coherent Motions in the Outer Region of Turbulent Boundary Layers," *Physics of Fluids,* Vol. 20, No. 10, Pt. II, Oct. 1977, pp. 124-132.

[12] Head, M. R. and Bandyopadhyay, P., "New Aspects of Turbulent Boundary Layer Structure," *Journal of Fluid Mechanics,* Vol. 107, 1981, pp. 297-338.

[13] Chen, P. and Blackwelder, R. F., "Large-Scale Motion in a Turbulent Boundary Layer: A Study Using Temperature Contamination," *Journal of Fluid Mechanics,* Vol. 89, Pt. 1, Nov. 1978, pp. 1-31.

[14] Brown, G. L. and Thomas, A. S. W., "Large Structure in a Turbulent Boundary Layer," *Physics of Fluids,* Vol. 20, No. 10, Pt. II, Oct. 1977, pp. 243-252.

[15] Zilberman, M., Wygnanski, I., and Kaplan, R. E., "Transition Boundary Layer Spot in a Fully Turbulent Environment," *Physics of Fluids,* Vol. 20, Oct. 1977, pp. 258-271.

[16] Wygnanski, I., "On Turbulent Spots," *Turbulence in Liquids,* University of Missouri, Rolla, Mo., 1981.

[17] Coles, D. and Barker, S. J., "Some Remarks on a Synthetic Turbulent Boundary Layer," *Turbulent Mixing in Non-reactive and Reactive Flows,* edited by S. N. B. Murthy, Plenum, New York, 1975, p. 285.

[18] Klebanoff, P. S., "Characteristics of Turbulence in a Boundary Layer with Zero Pressure Gradient," NACA TN 3178, 1954.

[19] Corke, T., Koga, D., Drubka, R., and Nagib, H., "A New Technique for Introducing Controlled Sheets of Smoke Streaklines in Wind Tunnels," *Proceedings of the ICIASF,* IEEE Publ. 77 CH1251-8 AES, 1977, p. 74.

[20] Wallace, J. M., Eckleman, H., and Brodkey, R. S., "The Wall Region in Turbulent Shear Flow," *Journal of Fluid Mechanics,* Vol. 54, Pt. 1, July 1972, pp. 39-48.

[21] Mumford, J. C., "The Structure of the Large Eddies in Fully Developed Turbulent Shear Flows. Pt. 1, The Plane Jet," *Journal of Fluid Mechanics,* Vol. 118, May 1982, pp. 241-268.

[22] Townsend, A. A., "Flow Patterns of large Eddies in a Wake and in a Boundary Layer," *Journal of Fluid Mechanics,* Vol. 95, Pt. 3, Dec. 1979, pp. 515-537.

[23] McClellan, J. H., Parks, T. W., and Rabiner, L. R., "FIR Linear Phase Filter Design Program," *Programs for Digital Signal Processing,* IEEE Press, New York, 1979.

[24] Rabiner, L. R. and Gold, B., *Theory and Application of Digital Signal Processing,* Prentice-Hall, Inc., New Jersey, 1975, pp. 472-478.

[25] Lynn, P. A., *An Introduction to the Analysis and Processing of Signals,* J. Wiley and Sons, New York, 1973.

[26] Corke, T. C., "A New View of Origin, Role and Manipulation of Large Scales in Turbulent Boundary Layers," Ph.D. Thesis, Illinois Institute of Technology, NASA CR 165861, 1981.

[27] Corke, T. C. and Nagib, H. M., "A New View on Origin, Role and Manipulation of Large Scales in Turbulent Boundary Layers," to be submitted to *Journal of Fluid Mechanics.*

[28] Rao, K., Narisimha, R., and Narayanan, M. A., "The Bursting Phenomenon in a Turbulent Boundary Layer," *Journal of Fluid Mechanics,* Vol. 48, Pt. 2, July 1971, pp. 334-352.

[29] Laufer, J. and Narayanan, M. A., "Mean Period of the Turbulent Production Mechanism in a Boundary Layer," *Physics of Fluids,* Vol. 14, Jan. 1971, p. 182.

[30] Black, T. J., "The Structure of Wall Turbulence," *Proceeding of the Heat Transfer and Fluid Mechanics Institute,* 1966, p. 366.

[31] Einstein, H. A. and Li, H., "The Viscous Sublayer Along a Smooth Boundary," ASCE Proceedings 82, 1956.

[32] Hanratty, T. J., "Turbulent Exchange of Mass and Momentum with a Boundary Layer," *Journal of the American Institute of Chemical Engineers,* Vol. 2, Sept. 1956, p. 359.

[33] Corke, T. C. and Nagib, H. M., "Unsteady Measurements in the Near Wall of Turbulent Boundary Layers," to be submitted to *Journal of Fluid Mechanics.*